Thermal properties of ^{16}O and ^{40}Ca with a realistic effective Hamiltonian

G. Bozzolo and J. P. Vary
Department of Physics, Iowa State University, Ames, Iowa 50011
(Received 1 October 1984)

A realistic microscopic effective nuclear Hamiltonian, H_{eff}, is employed with the spherical finite temperature Hartree-Fock approximation to evaluate the thermodynamic properties of ^{16}O and ^{40}Ca. We introduce a simple method to scale H_{eff} to accommodate the A-dependent effects. We then adjust the Hamiltonian slightly to reproduce appropriate ground state properties within spherical Hartree-Fock theory. A range of acceptable temperatures for each model space size can then be determined. The binding energy, free energy, density distributions, entropy, neutron and proton chemical potentials and single particle energies, occupation probabilities, and other properties are evaluated for temperatures $T \leq 7$ MeV. We provide convenient parametrizations for the excitation energy, rms radius, average density, and entropy as a function of T. We find the thermal response of these nuclei to be substantially greater than that obtained with zero range phenomenological forces.

I. INTRODUCTION

A realistic microscopically derived nuclear equation of state for finite nuclei would be of great utility for interpreting current experiments in heavy ion scattering and high energy particle-nucleus experiments. A first step towards obtaining this equation of state involves solving for the thermal properties of finite nuclei within a mean field approximation using a realistic Hamiltonian. In this paper we present results for two representative nuclei, ^{16}O and ^{40}Ca, in the spherical finite temperature Hartree-Fock approximation (FTHF) employing a realistic microscopic effective Hamiltonian.

A theoretical framework to explore the thermal properties of Fermion systems in the mean field approximation was first introduced by Bloch and de Domenicis.[1] This framework was applied to the reaction matrix at finite T and invoked for astrophysical problems.[2,3] Other studies of thermal properties of nuclear systems either postulated a single particle level scheme[4] or a phenomenological effective interaction.[5–11]

Recently, formal extensions to the mean field approach by Goodman[10] allow one to study critical properties of finite nuclei near the superfluid phase transition and as a function of angular momentum.[11] However, we are not aware of any calculations for the thermal properties of finite nuclei which have utilized a realistic Hamiltonian. It is our goal here to present details of our initial calculation of the microscopic Hamiltonian and its implementation within the finite temperature mean field framework. The current work amplifies and extends our earlier report.[12]

In later efforts we will explore the role of external constraints and fluctuations in order to obtain a more complete picture of the nuclear equation of state. Our work is similar in spirit to the work of the Giessen group[7] which employed a phenomenological Hamiltonian. While our initial effort here is limited in mass range and in size of the model space, we see many important differences in the thermal sensitivity of nuclei from the previously reported results. We provide evidence that these differences will remain in more extensive calculations.

We organize our paper so as to present in Sec. II a summary of the method of obtaining the microscopic effective Hamiltonian and our choices of restrictions in the problem such as model space details. We describe the scaling rules for the various components of the Hamiltonian and how they are obtained. In addition, we present the dynamical equations of the FTHF approximation. In Sec. III we describe how we adjust the Hamiltonian in a simple way to reproduce the ground state properties of these nuclei in the Hartree-Fock (HF) approximation and we give the theoretical motivation behind it. We proceed in Secs. IV and V to present the bulk of our results. Finally in Sec. VI we present our main conclusions and outlook for further work.

II. MICROSCOPIC STATISTICAL MODEL

Except for nuclei with $A \leq 3$, the bound state and quasibound state spectra of realistic Hamiltonians have not been exactly calculated. Therefore, numerous many-body formalisms with varying approximation schemes have been introduced and applied to finite nuclei. A thermal mean-field approach with phenomenological Hamiltonians has provided insight into the possible temperature (T) dependence of shell effects.[5–9] When addressing these issues with realistic Hamiltonians possessing strong short-range interactions we must either invoke a correlated basis or develop an effective interaction. We choose the latter.

The full Hamiltonian acting on all A nucleons is defined by

$$H = \sum_{i<j} h_{ij} = T_{\text{rel}} + V + V_C \ , \tag{2.1}$$

where its pure two-body nature is evident from the use of a relative kinetic energy operator

$$(T_{\rm rel})_{ij}=\frac{(\mathbf{p}_i-\mathbf{p}_j)^2}{2Am}\ , \tag{2.2}$$

the realistic nucleon-nucleon potential V, and the Coulomb potential V_C. We use $\mathbf{p}$ for single particle momentum and m for nucleon mass. Next we imagine that the many-body method we invoke is suitable to approximate the results of shell model diagonalization in a very large but finite basis. In particular, we choose a no-core basis space in order to avoid the need to calculate core polarization effects with realistic effective interactions. In previous applications with realistic effective no-core Hamiltonians we have used moment methods to obtain spectral distributions[13] and we have introduced[14] and applied[15] a coherent correlated pair method for the ground state energy as well as a recently developed dynamical basis generation scheme.[16] In the present effort we use the FTHF approximation in a sequence of no-core model spaces of increasing dimensionality. Since these many-body methods are assumed adequate for the particular applications where they are employed we only need to develop the effective Hamiltonian appropriate for diagonalization in the no-core basis space. We approximate the effective no-core Hamiltonian with

$$H_{\rm eff}=T_{\rm rel}+V_{\rm eff}+V_C\ . \tag{2.3}$$

In this approximation we neglect renormalization effects of $T_{\rm rel}$ and V_C and we calculate only leading order processes that contribute to $V_{\rm eff}$. We expect that these approximations become less severe as we increase the size of the no-core model space. In addition, we introduce phenomenological adjustments below which partially compensate for these approximations. The method of calculating the leading term of $V_{\rm eff}$,[17] which is the Brueckner G matrix[18] based on the Reid soft core potential,[19] has been presented elsewhere.[13,20,21] In recent efforts[13,15] we have also included the lowest order folded diagram in $V_{\rm eff}$ so that the diagrammatic representation of $V_{\rm eff}$ is now as shown in Fig. 1. Thus, besides higher order folded diagrams, we are only neglecting effective many-body forces between three or more particles. Our neglect of these higher order terms and the neglect of T-dependent effects on $H_{\rm eff}$ is based on the hope that model spaces may eventually be taken large enough and the many-body framework will become accurate enough that these corrections would be small.

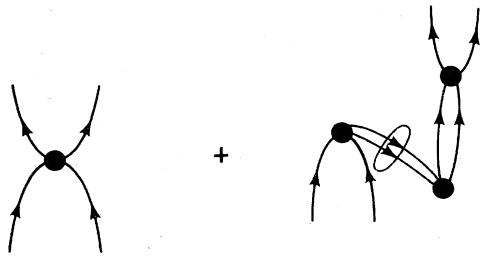

FIG. 1. Lowest order diagrams included in $V_{\rm eff}$ for no-core model spaces. The vertex represents an antisymmetric two-body G-matrix element based on a realistic nucleon-nucleon interaction. External lines and circled intermediate state lines represent states in the model space. The remaining intermediate pairs of states represent either one state in and one state out or both states out of the model space.

The matrix elements of $H_{\rm eff}$ are obtained in a harmonic oscillator basis with $\hbar\omega=14$ MeV. The terms in $V_{\rm eff}$ are obtained as a function of a gap parameter Ω, which specifies the energy difference between the last oscillator state of the model space at energy ϵ_L and the first state of the oscillator space above the model space at ϵ_F,

$$\epsilon_F-\epsilon_L=\hbar\omega+\frac{63-\Omega}{2}\ . \tag{2.4}$$

A strong dependence of the results on Ω would indicate sensitivity to the choice of model space. Here we employ Hamiltonians evaluated only for $\Omega=9$ MeV and explicitly demonstrate in Sec. III that the dependence of results on the choice of model space is weak in the low temperature regime.

In order to simplify applications of $H_{\rm eff}$ to as wide a range of nuclei as possible we have studied the dependence of the matrix elements of each term in Eq. (2.3) on the harmonic oscillator parameter $\hbar\omega$. All matrix elements of $T_{\rm rel}$ are exactly proportional to $(\hbar\omega)$, while all matrix elements of V_C are exactly proportional to $(\hbar\omega)^{1/2}$. We have studied the $\hbar\omega$ dependence of matrix elements of various short-range phenomenological nucleon-nucleon interactions. The larger two-body matrix elements are approximately proportional to $\hbar\omega$ due to the dominant role of relative s-state interactions. That is, the larger matrix elements of $V_{\rm eff}$ grow as the average distance between two nucleons decreases (depends on $\hbar\omega$) rather than growing as the volume decreases. Thus, if we signify a matrix element of an operator, e.g., $H_{\rm eff}$, by $\langle H_{\rm eff}\rangle$ implying it was calculated for A nucleons in an oscillator basis with spacing $\hbar\omega$, the matrix elements of $H_{\rm eff}$ in a basis with spacing $\hbar\omega'$ for A' nucleons are approximately given by

$$\langle H_{\rm eff}\rangle'=\frac{\hbar\omega'}{\hbar\omega}\left[\frac{A}{A'}\langle T_{\rm rel}\rangle+\langle V_{\rm eff}\rangle\right]+\left[\frac{\hbar\omega'}{\hbar\omega}\right]^{1/2}\langle V_C\rangle\ . \tag{2.5}$$

We have evaluated $H_{\rm eff}$ in a sequence of model spaces abbreviated as the two-space ($0s$, $0p$, and $1s$-$0d$ shells), the three-space (two-space plus $1p$-$0f$ shell), the four-space (three-space plus $2s$-$1d$-$0g$ shell), and the five-space (four-space plus $2p$-$1f$-$0h$ shell). This sequence of model spaces permits us to estimate convergence characteristics of the FTHF results for light nuclei.

We employ $H_{\rm eff}$ in the FTHF approximation which is to minimize the free energy

$$F=\langle H_{\rm eff}\rangle-TS\ , \tag{2.6}$$

where $\langle H_{\rm eff}\rangle$ is treated in the Hartree-Fock (HF) approximation with self-consistent thermal single-particle occupation probabilities.[7] That is, the basic approximation in FTHF is that the free energy depends only on the self-consistent thermal mean field.

In this way, one obtains a set of equations

$$h\,|\nu\rangle = e_\nu\,|\nu\rangle\ , \tag{2.7}$$

where $|\nu\rangle$ (e_ν) represents the HF single-particle state (energies) and h is given by its matrix elements

$$\langle\alpha\,|\,h\,|\beta\rangle = \sum_\gamma \langle\alpha\gamma\,|\,H_{\rm eff}\,|\beta\gamma\rangle f_\gamma\ . \tag{2.8}$$

Here, the thermal occupation probability for fermions is given by

$$f_\gamma = \left[1+\exp\left[\frac{e_\gamma-\mu}{T}\right]\right]^{-1}\ . \tag{2.9}$$

The chemical potentials μ are determined separately for neutrons and protons at each iteration by

$$\sum_{\substack{\nu\\ \text{neutrons}}} f_\nu = N \quad\text{and}\quad \sum_{\substack{\nu\\ \text{protons}}} f_\nu = Z\ . \tag{2.10}$$

The constraints (2.10) are the major difference between the application of a FTHF formalism to a finite versus an infinite system.

The entropy is obtained with

$$S = -\sum_\nu [f_\nu \ln(f_\nu)+(1-f_\nu)\ln(1-f_\nu)]\ , \tag{2.11}$$

and the thermal HF energy with

$$E_{\rm FTHF} = \sum_\alpha e_\alpha f_\alpha - \tfrac{1}{2}\sum_{\alpha<\beta}\langle\alpha\beta\,|\,H_{\rm eff}\,|\,\alpha\beta\rangle f_\alpha f_\beta\ . \tag{2.12}$$

We note that the full two-body density matrix $\rho^{(2)}$ has been approximated using the one-body density matrix $\rho^{(1)}$ by

$$\rho^{(2)}_{\alpha\beta\gamma\delta} = \rho^{(1)}_{\alpha\gamma}\rho^{(1)}_{\beta\delta} - \rho^{(1)}_{\alpha\delta}\rho^{(1)}_{\beta\gamma}\ . \tag{2.13}$$

This approximation was checked in Ref. 7 to verify that

$$T_r(\rho^{(2)}) = A(A-1) \tag{2.14}$$

holds to the 1% level in typical FTHF calculations.

We make a further approximation by restricting the FTHF orbitals to have good angular momentum, good total angular momentum and its projection, and good isospin projection. Only the radial wave function of the single-particle state is varied and we refer to this spherical Hartree-Fock (SHF) approximation since even-even nuclei will be spherically symmetric.

III. PHENOMENOLOGICAL ADJUSTMENTS AND RATIONALE

At $T=0$ we anticipated our SHF results would be similar to those of the Brueckner-Hartree-Fock (BHF) approximation.[22] Small differences may be ascribed to different choices for the Pauli operator [ours sets $Q=0$ for all pairs of single particle (s.p.) states in the model space] and s.p. spectra (we use oscillator energies) in the two-particle propagators of $V_{\rm eff}$. Indeed, we found the standard deficiencies in the $T=0$ solutions for ^{16}O and ^{40}Ca in the SHF approximation. Namely, we obtained too little binding but approximately correct rms radii. Our philosophy is to adjust $H_{\rm eff}$ in order to achieve agreement with measured ground state properties in the SHF approximation before proceeding with the FTHF calculations. To do this we simply introduce overall factors λ_1 and λ_2 for the kinetic energy and effective interaction terms, respectively, in $H_{\rm eff}$. We then adjust λ_1, λ_2, and $\hbar\omega$ simultaneously to achieve the desired rms radius and binding energy for a given nucleus within SHF for each choice of model space. We have chosen to adjust $H_{\rm eff}$ to produce a point nucleon mass rms radius in agreement with the measured charge rms radius in order to approximately compensate for the effects of spurious center of mass motion. One resulting set of parameters determined this way is given in Table I. These parameter sets are not unique and many nearly equivalent sets were easily obtained. We favored sets where λ_1 was less than but close to unity. We do this since $T_{\rm rel}$ is a positive definite operator and if we had renormalized it by itself into a finite model space this would have reduced its magnitude. Of course, in a more complete effective operator approach we cannot isolate the effect on separate components of H.

TABLE I. Overall factors λ_1 and λ_2 for the kinetic energy and effective interaction, respectively (see the text), and the appropriate value for $\hbar\omega$ for ^{16}O and ^{40}Ca in all three model spaces used in this work.

Nucleus	Model space	$\hbar\omega$	λ_1	λ_2
^{16}O	3	9.47	0.95	1.18
	4	9.40	0.97	1.26
	5	9.71	0.98	1.30
^{40}Ca	3	10.08	0.99	1.11
	4	7.95	0.98	1.22
	5	7.97	0.98	1.28

One might not expect $\hbar\omega$ to change smoothly when one adds a single shell at a time due to parity considerations. Instead, we expect changes to occur smoothly when viewed after a shell of each parity is added.

The behavior of λ_2 is especially noteworthy since it increases substantially with increasing model space. The fact that λ_2 is greater than unity compensates for the lack of sufficient binding observed even within BHF mentioned above. We also note that realistic Hamiltonians underbind nuclei even when employed with correlated wave functions, such as the coupled cluster or exp(S) formalism.[23] In fact, the BHF (Ref. 22) and exp(S) (Ref. 23) results both produce approximately 5 MeV/nucleon binding in ^{16}O for the Reid soft core interaction. The increase of λ_2 with model space increase is more subtle. As the model space increases, the renormalization procedure used to obtain $V_{\rm eff}$ produces an effective interaction with weaker attraction. As model spaces become very large the effective interaction approaches the bare interaction whose oscillator matrix elements are large and positive. Thus, our whole procedure of remaining within the HF approximation must break down eventually with increasing model spaces. Even though λ_2 becomes as large as 1.30 we see that model spaces have not yet increased to the point of losing the attraction in $V_{\rm eff}$. We feel the real test of our philosophy is whether the low temperature properties remain the same in the FTHF approximation with in-

TABLE II. Some representative ^{40}Ca matrix elements of $\lambda_2 V_{\text{eff}}$ in the $T=0$ spherical Hartree-Fock representation for different model spaces.

	J	T	Three-space	Four-space	Five-space
$\langle 0s_{1/2}0s_{1/2} \mid 0s_{1/2}0s_{1/2}\rangle$	0	1	−11.022	−11.016	−11.554
$\langle 0s_{1/2}0s_{1/2} \mid 0s_{1/2}0s_{1/2}\rangle$	1	0	−14.373	13.147	−12.817
$\langle 0s_{1/2}0s_{1/2} \mid 0p_{3/2}0p_{3/2}\rangle$	0	1	3.520	3.896	4.1772
$\langle 0s_{1/2}0s_{1/2} \mid 0p_{3/2}0p_{3/2}\rangle$	1	0	1.3312	1.5734	1.2693
$\langle 0s_{1/2}0s_{1/2} \mid 0p_{1/2}0p_{1/2}\rangle$	0	1	2.4833	2.7712	2.9717
$\langle 0s_{1/2}0s_{1/2} \mid 0p_{1/2}0p_{1/2}\rangle$	1	0	5.9897	5.4132	6.3309
$\langle 0s_{1/2}0s_{1/2} \mid 0d_{5/2}0d_{5/2}\rangle$	0	1	−0.3857	−0.9051	−0.9669
$\langle 0s_{1/2}0s_{1/2} \mid 0d_{5/2}0d_{5/2}\rangle$	1	0	0.3671	0.6632	0.8280
$\langle 0s_{1/2}0s_{1/2} \mid 1s_{1/2}1s_{1/2}\rangle$	0	1	−0.2271	−1.1907	−1.2611
$\langle 0s_{1/2}0s_{1/2} \mid 1s_{1/2}1s_{1/2}\rangle$	1	0	−0.2402	−1.6298	−1.6099
$\langle 0p_{3/2}0p_{3/2} \mid 0p_{3/2}0p_{3/2}\rangle$	0	1	−3.2593	−3.7622	−3.8001
$\langle 0p_{3/2}0p_{3/2} \mid 0p_{3/2}0p_{3/2}\rangle$	2	1	−2.7112	−2.4051	−2.6230
$\langle 0p_{3/2}0p_{3/2} \mid 0p_{3/2}0p_{3/2}\rangle$	1	0	−0.6324	−1.0672	−0.4582
$\langle 0p_{3/2}0p_{3/2} \mid 0p_{1/2}0p_{1/2}\rangle$	0	1	−5.6778	−5.6450	−6.1662
$\langle 0p_{3/2}0p_{3/2} \mid 0p_{1/2}0p_{1/2}\rangle$	1	0	2.4265	2.1063	2.1906
$\langle 0p_{3/2}0p_{3/2} \mid 0d_{5/2}0d_{5/2}\rangle$	0	1	0.8136	1.4841	1.3970
$\langle 0p_{3/2}0p_{3/2} \mid 0d_{5/2}0d_{5/2}\rangle$	2	1	0.9515	1.5744	1.6070
$\langle 0p_{3/2}0p_{3/2} \mid 0d_{5/2}0d_{5/2}\rangle$	1	0	−0.9629	−1.6223	−2.0769
$\langle 0p_{3/2}0p_{3/2} \mid 0d_{5/2}0d_{5/2}\rangle$	3	0	0.7134	1.1090	0.9705
$\langle 0p_{3/2}0p_{3/2} \mid 1s_{1/2}1s_{1/2}\rangle$	0	1	0.1359	0.1278	−0.0067
$\langle 0p_{3/2}0p_{3/2} \mid 1s_{1/2}1s_{1/2}\rangle$	1	0	−0.2918	−0.7179	−0.9343
$\langle 0d_{5/2}0d_{5/2} \mid 0d_{3/2}0d_{3/2}\rangle$	0	1	−1.4501	−0.8063	−0.7533
$\langle 0d_{5/2}0d_{5/2} \mid 0d_{3/2}0d_{3/2}\rangle$	2	1	−1.2408	−1.7858	−1.8372
$\langle 0d_{5/2}0d_{5/2} \mid 0d_{3/2}0d_{3/2}\rangle$	4	1	−0.5330	−0.79060	−0.8026
$\langle 0d_{5/2}0d_{5/2} \mid 0d_{3/2}0d_{3/2}\rangle$	1	0	0.1754	1.9000	2.2896
$\langle 0d_{5/2}0d_{5/2} \mid 0d_{3/2}0d_{3/2}\rangle$	3	0	−0.8644	−0.6792	−0.5822
$\langle 0d_{5/2}0d_{5/2} \mid 0d_{3/2}0d_{3/2}\rangle$	5	0	−3.4135	−4.6842	−4.6887
$\langle 0d_{5/2}0d_{5/2} \mid 1s_{1/2}1s_{1/2}\rangle$	0	1	−1.5894	−1.0945	−1.1164
$\langle 0d_{5/2}0d_{5/2} \mid 1s_{1/2}1s_{1/2}\rangle$	1	0	−0.5576	0.1852	0.3052
$\langle 0d_{5/2}0d_{5/2} \mid 0d_{3/2}0d_{3/2}\rangle$	0	1	−3.4625	−4.6549	−4.9006
$\langle 0d_{5/2}0d_{5/2} \mid 0d_{3/2}0d_{3/2}\rangle$	2	1	−0.6282	−0.7964	−0.8444
$\langle 0d_{5/2}0d_{5/2} \mid 0d_{3/2}0d_{3/2}\rangle$	1	0	1.8478	2.7594	2.8425
$\langle 0d_{5/2}0d_{5/2} \mid 0d_{3/2}0d_{3/2}\rangle$	3	0	0.2330	0.1931	0.1764
$\langle 1s_{1/2}1s_{1/2} \mid 1s_{1/2}1s_{1/2}\rangle$	0	1	−1.7576	−2.6205	−2.7019
$\langle 1s_{1/2}1s_{1/2} \mid 1s_{1/2}1s_{1/2}\rangle$	1	0	−2.1397	−2.9457	−2.8930
$\langle 1s_{1/2}1s_{1/2} \mid 0d_{3/2}0d_{3/2}\rangle$	0	1	−1.2977	−0.9344	−0.9744
$\langle 1s_{1/2}1s_{1/2} \mid 0d_{3/2}0d_{3/2}\rangle$	1	0	−0.7601	−1.4773	−1.5973

creasing model spaces. We show this to be true in Sec. IV.

We present in Table II some representative ^{40}Ca matrix elements for λ_2 V_{eff} in the $T=0$ SHF representation for different model spaces. One first notices that the matrix elements undergo large changes from one model space to the next. Furthermore, it is difficult to discern from these matrix elements any trend towards greater attraction or repulsion as the model space increases since the λ_2 factor has been included. However, the changes in proceedings from the four-space to the five-space are far less dramatic than the changes from the three-space to the four-space. This may be attributed to the fact that the three-space has only one major oscillator shell (the *f-p* shell) beyond the minimum needed for $N=Z=20$. The graduation in changes also suggests that calculations in larger model spaces could be useful.

We note in passing that we have introduced our phenomenological adjustments to H_{eff} to ensure that our $T=0$ properties are reasonably correct. We believe that the combination of theory and phenomenology yields an approach which has a reasonable chance of success in predicting the thermal properties correctly. We differ from the earlier FTHF efforts[5–11] primarily in that V_{eff} incorporates a tensor force and nonlocality effects. At the same time we do not have a contact three-body force. Any success achieved with our method at finite temperature may ultimately be attributed to choosing an H_{eff} which is more appropriate for calculating valence properties. That is, the low temperature thermal behavior of nuclei is sensitive to valence properties. To illustrate this point we refer ahead to Fig. 12 which shows the entropy distribution function in ^{40}Ca as a function of single-particle energy. It clearly demonstrates that for $T \leq 7$ MeV the entropy in FTHF is distributed among the orbitals immediately at the Fermi surface and hence it should be important to employ a V_{eff} which can be used with some confidence to predict the valence properties.

IV. TEMPERATURE DEPENDENCE OF GLOBAL PROPERTIES

The first major question to address is the model space dependence of the calculated thermal properties. We present in Figs. 2(a) and (b) the excitation energy E^* of ^{16}O and ^{40}Ca, respectively, as a function of T for the three-, four-, and five-spaces. We note three major features of these results. First, for $T \leq 3$ MeV the curves $E^*(T)$ are not significantly dependent on the model space for low T. Second, as one progresses to larger model spaces the expected parabolic dependence on T persists to progressively higher temperatures. Third, for $T \leq 1$ MeV, E^* is approximately constant.

The first two features signal the possibility that thermal properties calculated in limited model spaces will be approximately correct for $T \leq T_s$, where T_s is a model space dependent temperature. If "s" denotes the "three" in three-space for example, we estimate from the results in Figs. 2(a) and (b) and from other results below that for ^{16}O, in MeV, $T_3 \sim 4.5$, $T_4 \sim 5.75$, $T_5 \sim 7.0$ MeV and for ^{40}Ca, $T_3 \sim 3.0$, $T_4 \sim 5.0$, $T_5 \sim 7.0$ MeV. The somewhat smaller increments in T_s for ^{16}O may seem surprising but are consistent with the greater thermal response of ^{16}O than for ^{40}Ca which we present in more detail below. The inset displays the behavior of $E^*(T)$ at even higher T where model space limits are more severe.

Returning to the third feature we remark that for doubly magic nuclei the shell closure limits the thermal response for low T. However, we have restricted the variational problem to spherical symmetry and we believe that collective degrees of freedom could be very important at low T even for doubly magic nuclei. A separate effort will address this question.[24]

We parametrize the results in Figs. 2(a) and (b) by

$$E^*(T)=0, \quad T \leq T_0 ,$$
$$=\sigma(T-T_0)^2, \quad T > T_0 . \tag{4.1}$$

Then, with $T_0=1$ MeV we obtain $\sigma=0.185A$ for ^{16}O and $\sigma=0.104A$ for ^{40}Ca, where A represents the appropriate nucleon number. These results for ^{40}Ca follow the $\sigma=0.1A$ results of Sauer *et al.*[7] obtained for systems with $A \geq 40$ using phenomenological Hamiltonians. The larger thermal sensitivity of ^{16}O is clearly seen through his parametrization.

To further display the model space dependence of the results we show in Figs. 3(a) and (b) the rms radii of ^{16}O and ^{40}Ca, respectively. Here we portray results on an expanded scale where full scale represents approximately a 25% increase in rms radii. Features similar to those observed in Figs. 2(a) and (b) are found here. Note that due to the expanded scale, the three-space rms radius of ^{40}Ca differs from the four-space results at $T=3.0$ MeV by only 0.005 fm or by 0.14% even though the derivatives with T are quite different. Nevertheless, this result indicates we should avoid using the three-space for ^{40}Ca. In the remainder of this paper we present only five-space results for ^{16}O and ^{40}Ca and only for $T \leq 7$ MeV.

The rms radial expansion observed in Figs. 3(a) and (b) is considerably greater than reported by Sauer *et al.*[7] For

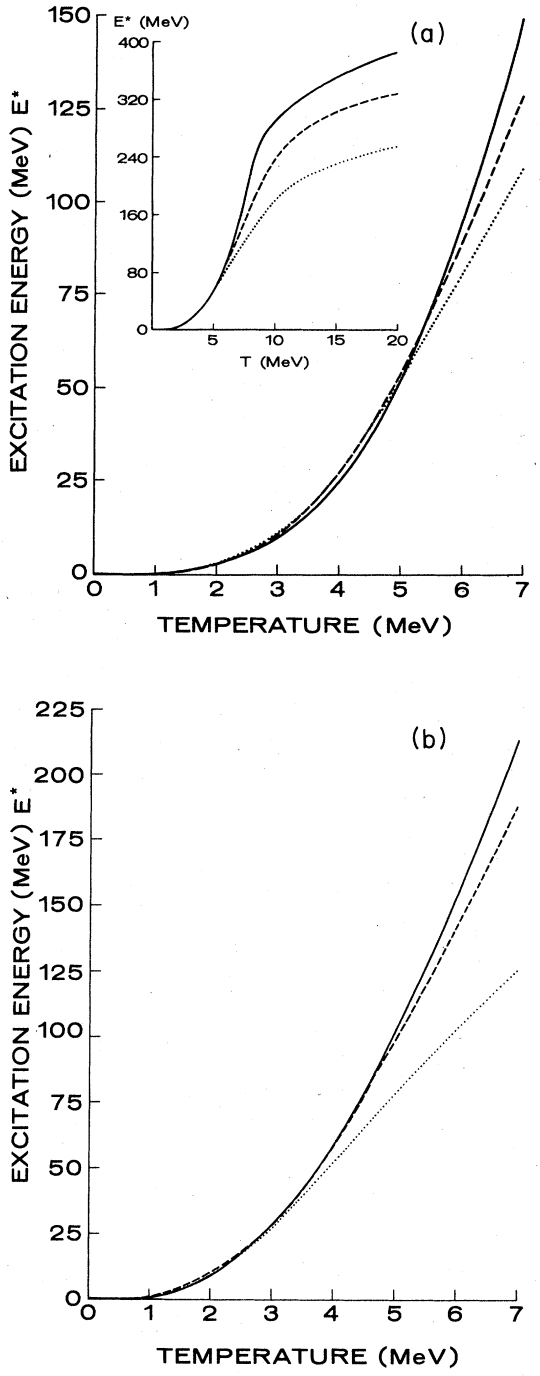

FIG. 2. (a) Excitation energy E^* as a function of nuclear temperature T for ^{16}O for different sizes of the model space. The dotted line indicates the three-space results, while the dashed and solid lines show the four- and five-space results, respectively. The inset also shows the excitation energy as a function of temperature for ^{16}O for a wider range of temperatures. (b) Excitation energy E^* as a function of nuclear temperature T for ^{40}Ca for different sizes of the model space. The dotted line indicates the three-space results, while the dashed and solid lines show the four- and five-space results, respectively.

example, at $T=5$ MeV we obtain $\sim 9\%$ (8%) radial expansion for ^{16}O (^{40}Ca), respectively, while Sauer *et al.* report virtually no radial expansion for ^{16}O and ^{40}Ca at $T=5$ MeV. Furthermore, the radial expansion becomes quadratically dependent on T so that a 31% and a 17% increase is observed at $T=7$ MeV for ^{16}O and ^{40}Ca, respectively.

We also conveniently parametrize the five-space results shown in Figs. 3(a) and (b) and obtain for the rms mass radii, $R(T)$,

$$R(T)=R_0(1+bT^2)\ , \tag{4.2}$$

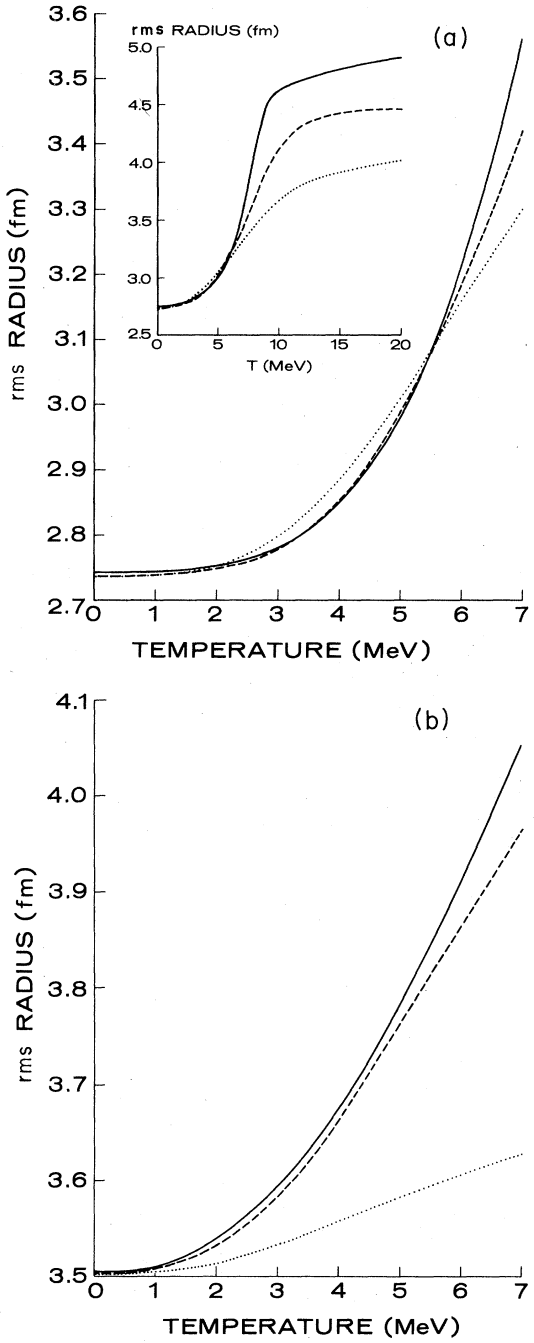

FIG. 3. (a) Root-mean-square radii as a function of temperature T for ^{16}O. The dotted line indicates the three-space results, while the dashed and solid lines show the four- and five-space results, respectively. The inset shows the same results but for a wider range of temperature. (b) Root-mean-square radii as a function of nuclear temperature for ^{40}Ca. The dotted line indicates the three-space results, while the dashed and solid lines show the four- and five-space results, respectively.

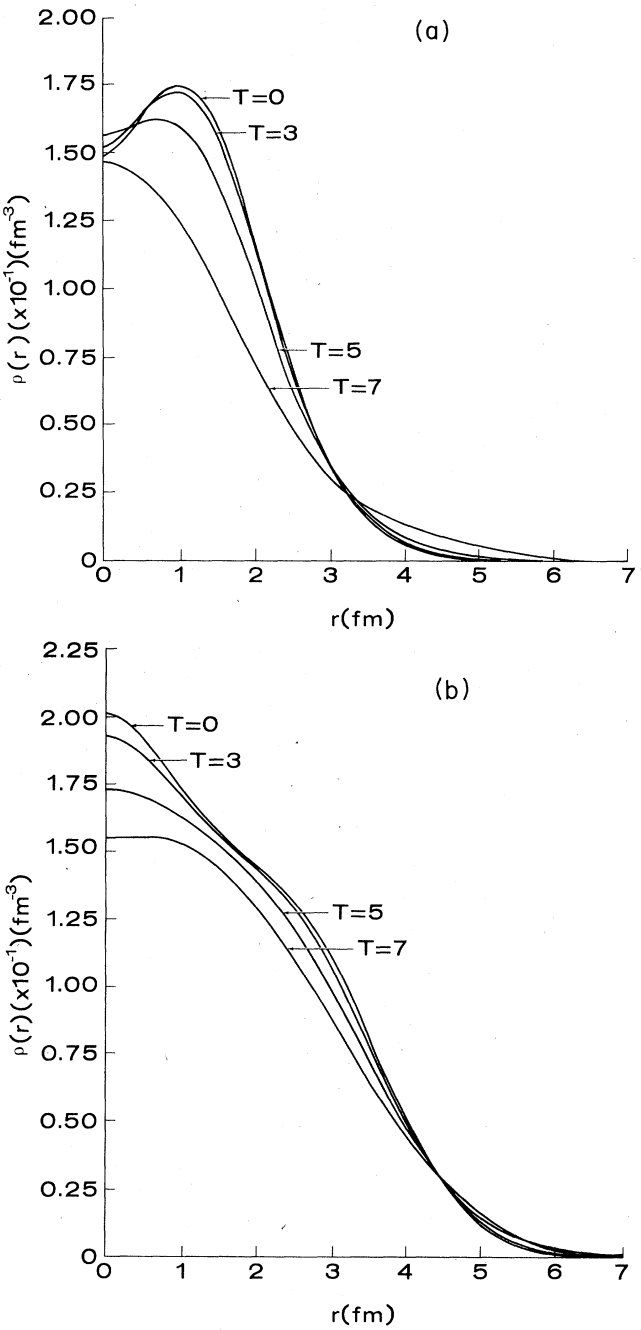

FIG. 4. (a) Radial density distribution for ^{16}O in the five-space for different nuclear temperatures. (b) Radial density distributions for ^{40}Ca in the five-space for different nuclear temperatures.

and we find $R_0=2.74$ (3.50) fm and $b=5.1\times10^{-3}$ (3.2×10^{-3}) MeV^{-2} for ^{16}O (^{40}Ca), respectively.

One may expect that the thermal response of ^{16}O is greater than the response of ^{40}Ca since orbitals near the Fermi surface are most sensitive to thermal excitation and a greater percentage of orbitals in ^{16}O are in the last filled shell at $T=0$ MeV than in ^{40}Ca. That is, 75% of the nucleons occupy the last filled shell in ^{16}O at $T=0$ MeV, while only 60% of the nucleons in ^{40}Ca are in the last filled shell at $T=0$ MeV. Since the last filled shell also contributes the most to the surface properties we may equally attribute the greater thermal response of ^{16}O to its greater surface to volume ratio. We return to this point when we discuss the entropy distribution in finite nuclei.

For a more complete picture of the thermal response we present in Figs. 4(a) and (b) the full radial mass distribution for ^{16}O and ^{40}Ca, respectively, at $T=0$, 3, 5, and 7 MeV. Again, no significant changes are evident for $0\le T\le3$ MeV. Between $T=3$ MeV and $T=7$ MeV both systems lose their low T features and have acquired a nearly Gaussian shape in their interior regions. We may parametrize the $T=7$ MeV results with

$$\rho_A(r,T=7)=A\left[\frac{3}{2\pi R^2}\right]^{3/2}\exp\left[-\frac{3r}{2R^2}\right]^2, \quad (4.3)$$

where R is the rms radius and equals 3.59 (4.06) fm for ^{16}O and ^{40}Ca, respectively, at this temperature.

For purposes of comparing results from these self-bound finite systems with infinite systems we present in Fig. 5 the average one-body density of these nuclei as a function of T. The average, $\bar{\rho}$, is given by

$$\bar{\rho}_T=\int_0^\infty[\rho_T(r)]^2d^3r\Big/\int_0^\infty\rho_T(r)d^3r\ . \quad (4.4)$$

From this information one may define an average volume V_T for the nucleus by $\bar{V}_T=A/\bar{\rho}_T$. Consistent with the results above we see that $\bar{\rho}_T$ decreases faster for ^{16}O than for ^{40}Ca.

For convenience we compare the calculated $\bar{\rho}$ with the estimate

$$\bar{\rho}'_T=\bar{\rho}_{T=0}\left[\frac{R_0}{R}\right]^3, \quad (4.5)$$

where R is given by the results of Figs. 3(a) and (b). We find this gives a reasonable parametrization over this range of T.

In Fig. 6 we plot the T-dependent contributions of neutrons and protons to the total entropy in ^{40}Ca. Little difference between neutron and proton contributions is observed. The expected linear dependence on T is obtained for $T\ge3$ MeV and is approximately observed for $1\le T\le3$ MeV, but with a different slope. If one fits the T dependence for $T>4$ MeV we obtain the entropy per nucleon quantities

$$\begin{aligned}S_n/N&=a_n+b_nT,\quad T>4\text{ MeV},\\ S_p/Z&=a_p+b_pT,\quad T>4\text{ MeV},\end{aligned} \quad (4.6)$$

with $(a_n,b_n,a_p,b_p)=(-1.08,\ 0.407,\ -1.25,\ 0.445)$ for ^{16}O and $(-0.396,\ 0.237,\ -0.381,\ 0.243)$ for ^{40}Ca.

The total free energy in Eq. (2.6) is minimized in these calculations with the approximation of a spherical mean field and subject to the condition of a chosen number of neutrons and protons. The resulting total free energy is plotted in Fig. 7 for ^{16}O and ^{40}Ca in the five-space as a function of T. In later applications we will search for

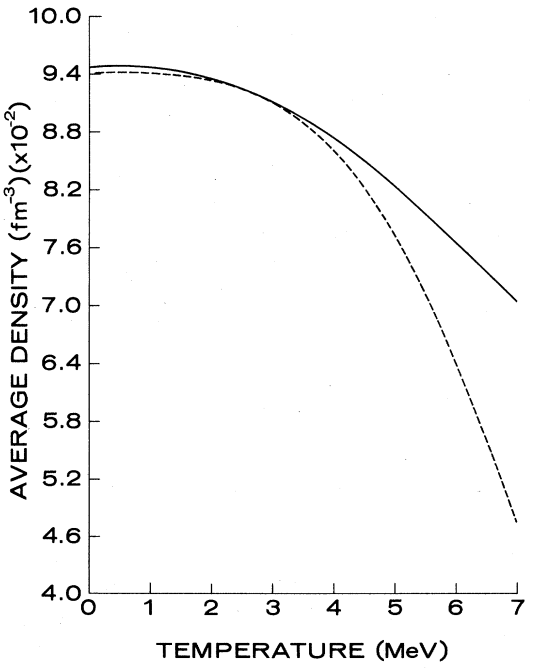

FIG. 5. Average density $\bar{\rho}$ (see the text) of ^{16}O and ^{40}Ca as a function of temperature.

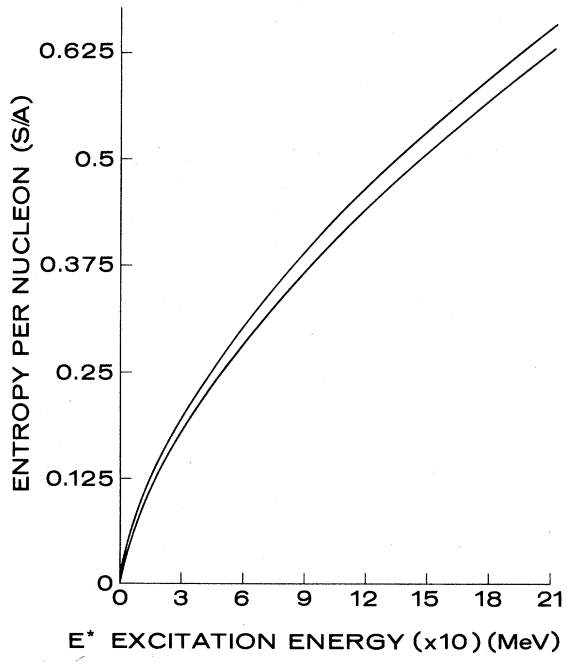

FIG. 6. Entropy per nucleon (for protons and neutrons) as a function of excitation energy for ^{40}Ca.

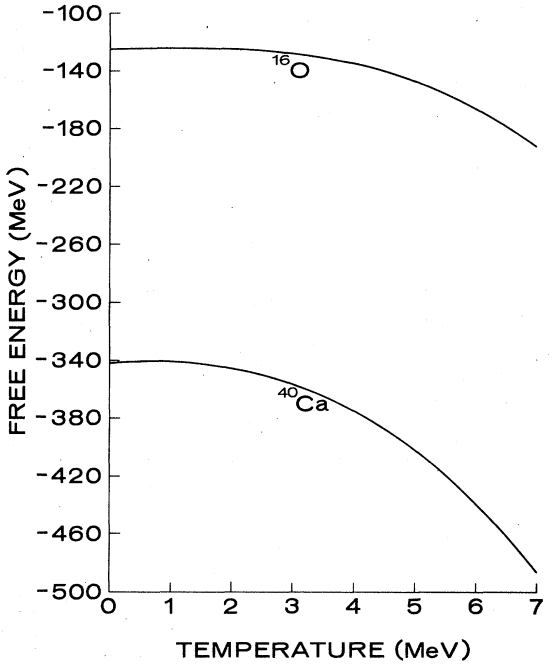

FIG. 7. Free energy as a function of temperature. Both curves (^{16}O and ^{40}Ca) were obtained in the five-space.

lower branches of these curves by relaxation of some of the symmetry constraints imposed here.[24]

We display in Fig. 8 the chemical potential for protons in ^{16}O and ^{40}Ca as a function of T. Similar curves with a small shift are obtained for the neutrons. For $T \geq 5$ MeV the proton chemical potentials fall at the same rate. However, for $0 \leq T \leq 5$ MeV substantially different T dependence is observed.

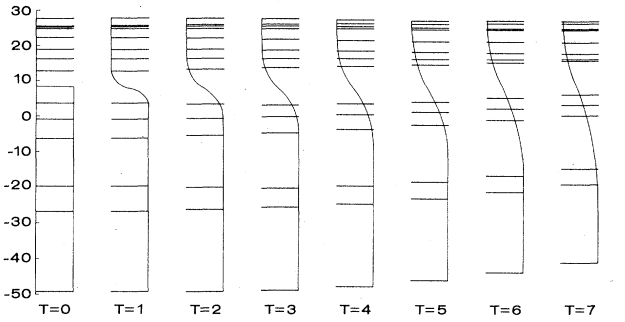

FIG. 9. Low-lying single-particle spectra for ^{40}Ca in the five-space for different nuclear temperatures. Superimposed is the Fermi occupation function [see Eq. (5.1)].

In concluding this section we note that the temperature dependence of all the global properties are substantially different between ^{16}O and ^{40}Ca. It is reasonable to attribute these differences to the differences in the fraction of nucleons in the last filled shell at $T=0$ or, equivalently, to differences in the surface to volume ratio. However, to substantiate this connection we need to examine more nuclei in the FTHF approximation. A convincing demonstration of the dependence of thermal properties on surface, volume, and shell properties combined will require the more careful parametrization of these results and

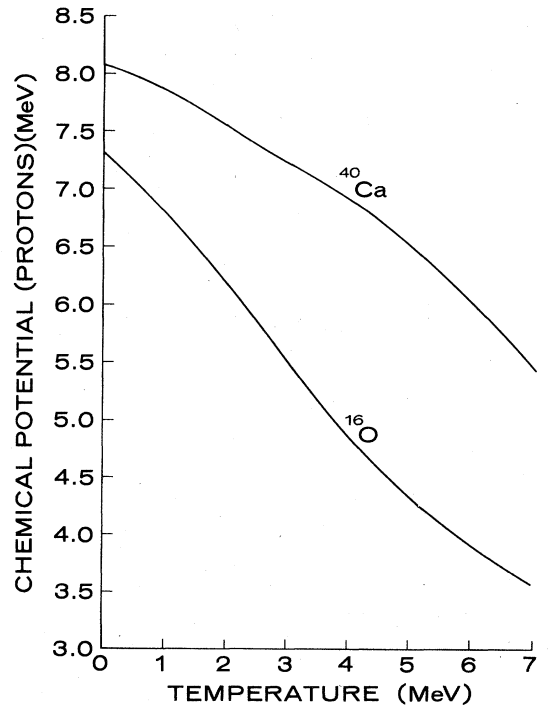

FIG. 8. Chemical potential for protons as a function of temperature. Both curves (^{16}O and ^{40}Ca) were obtained in the five-space.

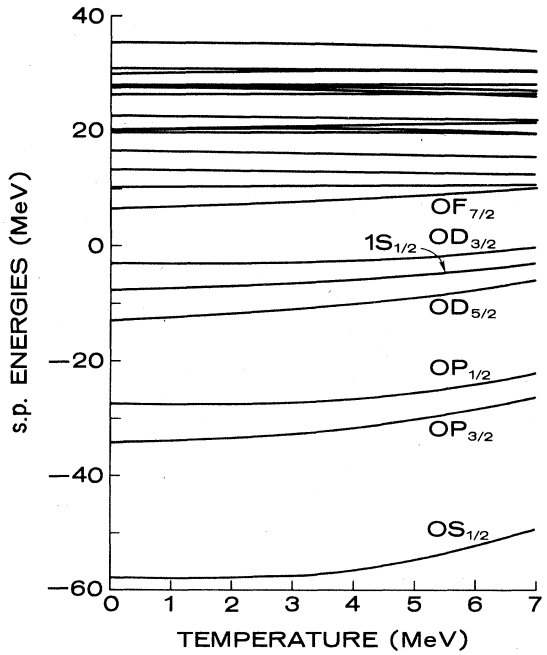

FIG. 10. Single-particle neutron states as a function of nuclear temperature for ^{40}Ca in the five-space. The unlabeled levels are approximately consistent with the expected shell-model ordering at $T=0$ MeV.

TABLE III. Single-particle energies of neutrons and protons for ^{40}Ca in the five-space and for different values of the temperature T. The first two columns show the l and $2j$ values of the corresponding single particle states.

		$T=0$		$T=2$		$T=4$		$T=6$		$T=8$	
l	$2j$	Neutrons	Protons	Neutrons	Protons	Neutrons	Protons	Neutrons	Protons	Neutrons	Protons
0	1	−57.939	−49.351	−58.019	−49.411	−56.533	−48.000	−52.342	−44.014	−46.113	−38.071
1	3	−34.482	−26.821	−34.032	−26.339	−32.296	−24.640	−28.900	−21.395	−24.045	−16.783
1	1	−27.431	−19.632	−27.942	−20.101	−27.544	−19.734	−24.467	−16.828	−19.718	−12.348
2	5	−13.073	−6.2499	−12.284	−5.4559	−10.450	−3.6603	−7.8717	−1.1892	−4.6511	1.8358
0	1	−7.7456	−0.9428	−7.4233	−0.6257	−6.2661	0.4977	−4.3593	2.2658	−2.0948	4.2720
2	3	−3.1331	3.7725	−3.5030	3.4467	−3.3817	3.5773	−1.6763	5.1527	0.7613	7.3328
3	7	6.2401	12.627	6.8799	13.240	7.9688	14.218	9.0916	15.150	10.418	16.209
1	3	10.102	16.225	10.298	16.390	10.398	16.355	10.371	16.095	10.532	15.996
1	1	13.100	18.942	13.094	18.932	12.730	18.506	12.308	17.909	12.177	17.562
3	5	16.399	22.364	16.088	22.103	15.477	21.493	15.194	21.041	15.221	20.811
0	1	19.603	24.849	19.723	24.964	19.633	24.870	19.255	24.504	19.105	24.395
4	9	19.988	25.483	20.424	25.903	20.888	26.326	21.016	26.380	21.222	26.484
2	5	20.096	25.387	20.250	25.532	20.149	25.399	19.647	24.856	19.322	24.510
2	3	22.363	27.750	22.367	27.740	22.122	27.469	21.719	27.064	21.592	26.975
1	3	25.998	31.297	26.132	31.431	26.225	31.539	26.203	31.560	26.464	31.880
3	7	27.247	32.280	27.351	32.457	26.827	32.337	26.109	31.569	25.544	30.919
4	7	27.471	33.001	27.418	32.879	27.392	32.441	27.031	32.100	26.904	32.021
1	1	27.744	33.338	27.797	33.380	27.679	33.235	27.593	33.161	27.914	33.517
5	11	29.794	34.922	30.068	35.186	30.218	35.299	28.881	35.008	29.777	34.724
4	5	30.701	36.329	30.599	36.188	30.381	35.920	30.268	35.821	30.459	36.042
5	9	35.333	40.460	35.328	40.452	34.940	40.048	34.160	39.228	33.415	38.422

those of the next section in terms of a thermal liquid drop model plus shell corrections.[25]

V. TEMPERATURE DEPENDENCE OF SINGLE-PARTICLE PROPERTIES

We proceed with a presentation of a selected set of results for the thermal single-particle (s.p.) properties. Here again we restrict ourselves to the five-space results.

In Fig. 9 we present the lowest 14 proton FTHF single-particle energies (s.p.e.) of ^{40}Ca at integral values of T from 0 to 7 MeV. Superimposed is a plot of the fermion occupation function

$$f(e)=\left[1+\exp\left[\frac{e-\mu}{T}\right]\right]^{-1} \tag{5.1}$$

which uses the self-consistently determined value of μ at each T. Although the most deeply bound orbitals are not significantly depopulated, their s.p.e. change considerably. This sensitivity of the s.p.e. contrasts sharply with the results of Sauer *et al.*,[7] who reported the s.p.e. virtually unchanged for $T \leq 5$ MeV.

An easy way to see this thermal sensitivity is found in Fig. 10 which portrays the continuous change in neutron s.p.e. with T for ^{40}Ca. Table III shows numerical values of the ^{40}Ca s.p.e. both for protons and neutrons. The most striking feature here is that the spin-orbit splitting dissolves fast enough that the gap between the highest orbit of one shell and the lowest orbit of the next is actually preserved out to $T \sim 7$ MeV. Of course, the splitting between shell centroids is decreasing with T as is expected.

We underscore the character of these results by recalling that these self-consistent T-dependent neutron s.p.e. arise solely from the mean field of a pure two-body effective Hamiltonian. Since there is no input s.p. Hamiltonian the spin-orbit splitting and its T dependence are due to the effective two-body interaction alone.

The occupation probabilities of the proton orbitals in ^{40}Ca are presented in Fig. 11 as a function of T. The most significant changes occur for orbitals closest to the Fermi surface. Both the deeply bound and the highest orbitals occupation probabilities barely deviate from their $T=0$ values.

VI. CONCLUSION AND OUTLOOK

We conclude the presentation of results by considering the entropy as a continuous function of $f(e)$, that is,

$$S(e)=-\{f(e)\ln[f(e)]+[1-f(e)]\ln[1-f(e)]\}\ , \tag{6.1}$$

where $f(e)$ is given by Eq. (5.1). Then, we use the chemical potential determined self-consistently for the proton orbitals in ^{16}O and plot $S(e)$ vs e in Fig. 12 at $T=1$, 3, 5, and 7 MeV. This illustrates the range of s.p.e. most important for the thermal response of nuclei at each T. Clearly, the thermal valence properties play a dominant role in the results we obtain. Consequently, we argue that the greater thermal response of ^{16}O and ^{40}Ca is a firm prediction of our method and is in sharp contrast with the results of Sauer *et al.*[7] The greater thermal response is due to our choice of a realistic microscopic effective Hamiltonian, which should be more reliable for the valence properties of these systems.

All the results we have presented are limited to the spherical thermal mean field approximation. Numerous

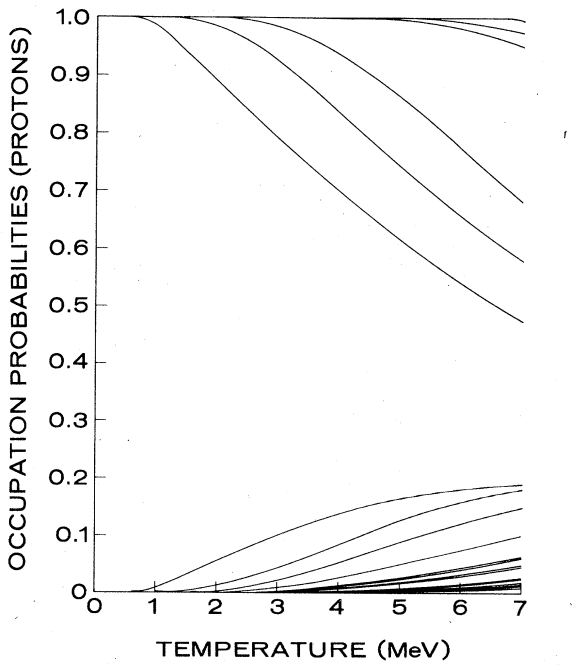

FIG. 11. Occupation probabilities for protons as a function of nuclear temperature for ^{40}Ca in the five-space.

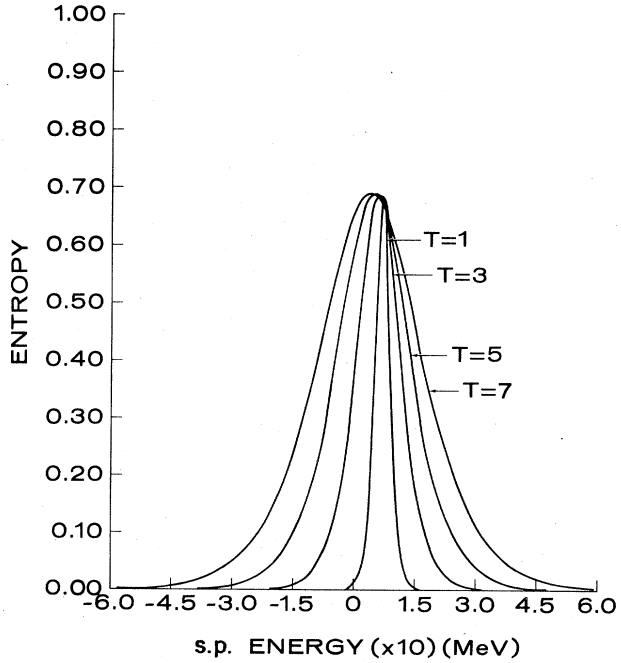

FIG. 12. Entropy as a continuous function of single-particle energy for ^{40}Ca in the five-space, for different values of the temperature.

extensions and improvements may be incorporated in a straightforward manner. For example, at low temperature it will be important to investigate the role of deformations.[24]

With constraints introduced into the variational treatment one may simultaneously explore the equation of state with external pressure and the role of fluctuations in regions of critical behavior.

Finally, we remark that it is also straightforward to develop microscopic thermal approaches to finite nuclei which treat short-range correlations and long-range correlations more completely.[26]

ACKNOWLEDGMENTS

We thank Alan Goodman, Osvaldo Civitarese, Hank Miller, Phil Siemens, and Angel Plastino for useful discussions. One of us (J.P.V.) wishes to acknowledge the hospitality of the Council of Scientific and Industrial Research—National Research Institute for Mathematical Sciences (CSIR—NRIMS) Pretoria, where part of this work was completed. This work was supported by the Director, Office of Energy Research, Division of Nuclear Physics of the Office of High Energy and Nuclear Physics of the U.S. Department of Energy under Contract DE-AC02-82-ER40068.

[1]C. Bloch and C. de Dominicis, Nucl. Phys. **7**, 459 (1958).
[2]J. R. Buehler and S. A. Coon, Astrophys. J. **212**, 807 (1977).
[3]See, J. Robert Buchler and Bhaskar Datta, Phys. Rev. C **19**, 494 (1979) for a critique of approximate treatments of the T dependence of the effective interaction.
[4]V. S. Ramamurthy, S. S. Kapoor, and S. K. Kataria, Phys. Rev. Lett. **25**, 386 (1970); L. G. Moretto, Nucl. Phys. **A182**, 641 (1972); J. R. Huizenga and L. G. Moretto, Annu. Rev. Nucl. Sci. **22**, 427 (1972); A. S. Jensen and J. Damgaard, Nucl. Phys. **A210**, 282 (1973); T. Dossing and A. S. Jensen, *ibid.* **A222**, 493 (1974).
[5]M. Brack and P. Quentin, Phys. Lett. **52B**, 159 (1974).
[6]M. Brack and P. Quentin, Phys. Scr. **10A**, 163 (1974).
[7]U. Mosel, P. G. Zint, and K. H. Passler, Nucl. Phys. **A236**, 252 (1974), and references therein; G. Sauer, H. Chandra, and U. Mosel, *ibid.* **A264**, 221 (1976), and references therein.
[8]P. Quentin and H. Flocard, Annu. Rev. Nucl. Sci. **28**, 523 (1978).
[9]M. Brack and P. Quentin, Nucl. Phys. **A361**, 35 (1981).
[10]A. Goodman, Nucl. Phys. **A352**, 30 (1981).
[11]A. Goodman, Nucl. Phys. **A402**, 189 (1983).
[12]G. Bozzolo and J. P. Vary, Phys. Rev. Lett. **53**, 903 (1984).
[13]F. J. Margetan and J. P. Vary, Phys. Rev. C **28**, 907 (1983).
[14]J. P. Vary and A. Plastino, Phys. Rev. C **28**, 2494 (1983); A. Klar, F. J. Margetan, J. P. Vary, and A. Plastino, *ibid.* **28**, 2499 (1983).
[15]G. Bozzolo, A. Klar, and J. P. Vary, Phys. Rev. C **29**, 1069 (1984).
[16]G. Bozzolo, J. P. Vary, and A. Plastino, Phys. Rev. C **31**, 207 (1985).
[17]B. H. Brandow, Rev. Mod. Phys. **39**, 771 (1967).
[18]K. A. Brueckner, Phys. Rev. **97**, 1353 (1955).
[19]R. V. Reid, Ann. Phys. (N.Y.) **50**, 411 (1968).
[20]J. P. Vary, in *Theory and Application of Moment Methods in Many-Fermion Systems,* edited by B. J. Dalton, S. M. Grimes, J. P. Vary, and S. A. Williams (Plenum, New York, 1980).
[21]J. P. Vary and S. N. Yang, Phys. Rev. C **15**, 1545 (1977).
[22]K. T. R. Davies and R. J. McCarthy, Phys. Rev. C **4**, 81 (1971), and references therein.
[23]H. Kümmel, K. H. Lürhmann, and J. G. Zabolitzky, Phys. Rep. **36C**, 1 (1978), and references therein.
[24]G. Bozzolo, H. G. Miller, and J. P. Vary (unpublished).
[25]G. Bozzolo, O. Civitarese, and J. P. Vary (unpublished).
[26]R. A. Broglia, O. Civitarese, C. H. Dasso, and A. Winther, Phys. Lett. **B73**, 405 (1978); O. Civitarese, S. Furui, M. Ploszajczak, and Amond Faessier, Nucl. Phys. **A408**, 61 (1983); O. Civitarese, G. G. Dussel, and R. P. J. Perazzo, *ibid.* **A404**, 15 (1983).